BBA - Molecular Basis of Disease 1865 (2019) 206–217

Contents lists available at ScienceDirect

BBA - Molecular Basis of Disease

journal homepage: www.elsevier.com/locate/bbadis

Inhibition of CYP2E1 attenuates myocardial dysfunction in a murine model of insulin resistance through NLRP3-mediated regulation of mitophagy

Jun Ren[a,b,*,1], Zhaohui Pei[c,1], Xiyao Chen[b], Melissa J. Berg[b], Khalid Matrougui[d], Qing-hua Zhang[e,**], Yingmei Zhang[a,b,*]

[a] Department of Cardiology, Zhongshan Hospital Fudan University, Shanghai 210032, China
[b] Center for Cardiovascular Research and Alternative Medicine, University of Wyoming College of Health Sciences, Laramie, WY 82071, USA
[c] The Second Department of Cardiology, The Third Hospital of Nanchang, Nanchang, Jiangxi 330009, China
[d] Department of Physiology, Eastern Virginia School of Medicine, Norfolk, VA, USA
[e] Department of Obstetrics and Gynecology, Daping Hospital, Third Military Medical University, Chongqing 400038, China

ARTICLE INFO

Keywords:
CYP2E1
Insulin resistance
Cardiac function
Mitophagy
NLRP3
iNOS

ABSTRACT

Insulin resistance leads to myocardial contractile dysfunction and deranged autophagy although the underlying mechanism or targeted therapeutic strategy is still lacking. This study was designed to examine the impact of inhibition of the cytochrome P450 2E1 (CYP2E1) enzyme on myocardial function and mitochondrial autophagy (mitophagy) in an Akt2 knockout model of insulin resistance. Adult wild-type (WT) and $Akt2^{-/-}$ mice were treated with the CYP2E1 inhibitor diallyl sulfide (100 mg/kg/d, i.p.) for 4 weeks. Cardiac geometry and function were assessed using echocardiographic and IonOptix systems. Western blot analysis was used to evaluate autophagy, mitophagy, inducible NOS (iNOS), and the NLRP3 inflammasome, a multi-protein intracellular pattern recognition receptor complex. Akt2 deletion triggered insulin resistance, compromised cardiac contractile and intracellular Ca^{2+} property, mitochondrial ultrastructural damage, elevated $O2^{-}$ production, as well as suppressed autophagy and mitophagy, accompanied with elevated levels of NLRP3 and iNOS, the effects of which were significantly attenuated or ablated by diallyl sulfide. *In vitro* studies revealed that the NLRP3 activator nigericin nullified diallyl sulfide-offered benefit against Akt2 knockout on cardiomyocyte mechanical function and mitophagy (using Western blot and colocalization of GFP-LC3 and MitoTracker Red). Moreover, inhibition of iNOS but not mitochondrial ROS production attenuated Akt2 deletion-induced activation of NLRP3, substantiating a role for iNOS-mediated NLRP3 in insulin resistance-induced changes in mitophagy and cardiac dysfunction. In conclusion, these data depict that insulin resistance through CYP2E1 may contribute to the pathogenesis of myopathic changes including myocardial contractile dysfunction, oxidative stress and mitochondrial injury, possibly through activation of iNOS and NLRP3 signaling.

1. Introduction

Insulin plays a pivotal role in the regulation of myocardial oxidative phosphorylation and contractile function [1]. Resistance to insulin signaling is a cardinal feature of type 2 diabetes and is associated with multiple cardiovascular and metabolic diseases including cardiac dysfunction manifested as disruption of cardiac geometry, myofibrillary architecture and contractile function [2–4]. Although several scenarios have been put forward for insulin resistance-induced cardiac pathological sequelae including inflammation, endoplasmic reticulum, dyslipidemia and oxidative stress [5–9], the precise mechanism behind cardiac anomalies under insulin resistance remains elusive, making target therapeutics against insulin resistance-induced cardiomyopathy somewhat challenging. Insulin signaling is controlled by a cascade of complex signaling components with the phosphatidylinositol 3-kinase (PI3K)-Akt axis mainly controlling insulin-mediated metabolic flexibility [10,11]. Impaired PI3K/Akt signaling is documented in a number of pathological conditions accompanied with insulin resistance, obesity, and type 2 diabetes [12–15]. In particular, mutation of Akt2 (R274H) was shown to lead to severe hyperinsulinemia and diabetes in human subjects [16], consistent with the development of insulin resistance with Akt2 knockout in mice [17,18]. These findings consolidate a

* Corresponding authors at: Department of Cardiology, Zhongshan Hospital Fudan University, Shanghai 200032, China.
** Corresponding author.
E-mail addresses: jren@uwyo.edu (J. Ren), zhangqh1123@163.com (Q.-h. Zhang), zhangym197951@126.com (Y. Zhang).
[1] Equal contribution.

https://doi.org/10.1016/j.bbadis.2018.08.017
Received 28 April 2018; Received in revised form 2 August 2018; Accepted 10 August 2018
Available online 16 August 2018
0925-4439/

permissive role for Akt2 in metabolic regulation.

Recent proteomic and transcriptomic analyses have revealed significantly altered levels of metabolic genes in insulin resistance and type 2 diabetes mellitus including aldehyde dehydrogenase (ALDH) and cytochrome P450 2E1 (CYP2E1) [19–21]. CYP2E1 is a ROS generating enzyme with a proven role in metabolic diseases [21,22]. CYP2E1 was demonstrated to be involved in isoproterenol-induced cardiac dysfunction [23] although evidence for a role of CYP2E1 in insulin resistance is still lacking. Given the pivotal role of CYP2E1 in metabolism and oxidative stress [21,22], this study was designed to examine the effect of the CYP2E1 inhibitor diallyl sulfide on insulin resistance-induced myocardial contractile dysfunction, intracellular Ca^{2+} derangement and potential signaling mechanisms involved with a focus on autophagy in particular mitochondrial autophagy, which is known to play a major role in insulin resistance [24]. Superoxide (O_2^-) levels were monitored as an indicator for oxidative stress. As an essential member of the nucleotide-binding oligomerization domain-like receptor family, the pyrin domain-containing 3 (NLRP3) inflammasome plays an important role in the pathogenesis of various disorders including diabetes, insulin resistance and other metabolic disorders [25,26]. To examine the possible involvement of NLRP3 signaling in Akt2 knockout-induced insulin resistance, levels of NLRP3 were evaluated in myocardium from WT and Akt2$^{-/-}$ mice with or without diallyl sulfide treatment. Given that type 2 diabetes and insulin resistance are closely linked with excessive activation of inducible NOS (iNOS) [27], levels of iNOS were also scrutinized. Activation of iNOS leads to mitochondrial damage and ROS production [27,28], and more recently activation of NLRP3 inflammasome [29,30]. However, the potential involvement of iNOS and NLRP3 in insulin resistance- and CYP2E1 inhibition-induced myocardial response remains unknown. To further discern the role of iNOS, NLRP3 and mitochondrial integrity (mitophagy) in Akt2 ablation- and diallyl sulfide-induced cardiac contractile responses, *in vitro* studies were performed using selective pharmacological inhibitors in adult or neonatal murine cardiomyocytes isolated from WT and Akt2$^{-/-}$ mice.

2. Materials and methods

2.1. Akt2 knockout (Akt2$^{-/-}$) mice and intraperitoneal glucose tolerance test (IPGTT)

All animal procedures were approved by the Animal Care and Use Committees at the Zhongshan Hospital Fudan University (Shanghai, China) and the University of Wyoming (Laramie, WY, USA). In brief, Akt2 knockout (Akt2$^{-/-}$) mice were obtained from Dr. Morris Birnbaum at the University of Pennsylvania (Philadelphia, PA, USA) and were characterized in our lab previously [31]. A cohort of adult (12-month-old) WT and Akt2$^{-/-}$ mice were administered the CYP2E1 inhibitor diallyl sulfide (100 mg/kg/d, i.p.) for 4 weeks [32,33]. Prior to sacrifice, mice fasted for 12 h were given an injection of glucose (2 g/kg b.w., i.p.). Blood samples were collected prior to glucose challenge, as well as 30, 60, 90 and 120 min thereafter. Blood glucose levels were determined using an Accu-Chek III glucose analyzer. The area under the curve (AUC) was calculated using trapezoidal analyses for each adjacent time point and blood glucose level [34].

2.2. p-Nitrophenol hydroxylation activity

Formation of 4-nitrocatechol from p-Nitrophenol (p-NP) hydroxylation was employed as indicator for CYP2E1 activity. In brief, tissue samples were incubated in 0.1 M phosphate buffer containing 1.3 nmol/ml P450, 1 mM NADPH, and 100 μM p-NP with a total volume of 0.5 ml (pH 7.5 at 37 °C). A 30-min reaction was initiated and terminated by adding NADPH and 10% perchloric acid, respectively. The mixture was cooled on ice, and proteins were removed by centrifugation at 15,000 × *g* for 10 min. NaOH (100 mM, 30 μl) was added to supernatants (300 μl), and absorbance was read at 540 nm using a Spectrometer [35].

2.3. Echocardiographic assessment

Cardiac geometry and function were evaluated in anesthetized (ketamine 80 mg/kg & xylazine 12 mg/kg, i.p.) mice using a 2-D guided M-mode echocardiography (Sonos 5500) equipped with a 15–6 MHz linear transducer. Left ventricular (LV) wall, septum and chamber dimensions during diastole and systole were recorded from 3 consecutive cycles in M-mode. Fractional shortening was calculated from LV end-diastolic (EDD) and end-systolic (ESD) diameters using the equation (EDD-ESD)/EDD. Heart rate was calculated from 10 consecutive cardiac cycles [34].

2.4. Cardiomyocyte isolation and in vitro drug treatment

After ketamine/xylazine (80 and 12 mg/kg, respectively, i.p.) sedation, hearts were removed and perfused with KHB buffer containing (in mM): 118 NaCl, 4.7 KCl, 1.2 $MgSO_4$, 1.2 KH_2PO_4, 25 $NaHCO_3$, 10 HEPES and 11.1 glucose. Hearts were digested with Liberase for 20 min. Left ventricles were removed and minced before being filtered. Cardiomyocyte yield was ~75% which was not affected by either Akt2 ablation or diallyl sulfide. Only rod-shaped cardiomyocytes with clear edges were used for mechanical evaluation [36]. To examine the role of NLRP3 on diallyl sulfide-induced cardiac response, cardiomyocytes from WT and Akt2$^{-/-}$ mice were treated with diallyl sulfide (100 μM) [37] at 37 °C for 6 h in the absence or presence of the specific NLRP3 activator nigericin (20 μM) [38] prior to the assessment of the mitophagy marker Parkin and mechanical function. To examine the role of iNOS and mitochondrial ROS in NLRP3 signaling, cardiomyocytes from WT and Akt2$^{-/-}$ mice were treated with selective iNOS inhibitor S-ethyl-isothiourea (SEITU, 1 μM) [29] or the mitochondrial ROS scavenger MitoQ (2 μM) [29] at 37 °C for 6 h prior to the assessment of NLRP3.

2.5. Cell shortening/relengthening

Mechanical properties of cardiomyocytes were assessed using a SoftEdge MyoCam® system (IonOptix Corporation, Milton, MA, USA). Cells were placed in a chamber mounted on the stage of an inverted microscope (Olympus, IX-70) and superfused (~1 ml/min at 25 °C) with a buffer containing (in mM): 131 NaCl, 4 KCl, 1 $CaCl_2$, 1 $MgCl_2$, 10 glucose, 10 HEPES, at pH 7.4. The cells were field stimulated with supra-threshold voltage at a frequency of 0.5 Hz. The myocyte being studied was displayed on the computer monitor using an IonOptix MyoCam camera. An IonOptix SoftEdge software was used to capture changes in cell length during shortening and relengthening. Cell shortening and relengthening were assessed using the following indices: peak shortening (PS) — indicative of ventricular contractility, time-to-PS (TPS) — indicative of contraction duration, time-to-90% relengthening (TR_{90}) — represents relaxation duration, and maximal velocities of shortening (+ dL/dt) and relengthening (− dL/dt) — indicatives of maximal velocities of ventricular pressure rise/fall [34].

2.6. Intracellular Ca^{2+} transients

Cardiomyocytes were loaded with fura-2/AM (0.5 μM) for 15 min, and fluorescence intensity was measured with a dual-excitation fluorescence photomultiplier system (IonOptix). Myocytes were placed on an inverted Olympus microscope and imaged through a Fluor 40 ×-oil objective. Cells were exposed to light emitted by a 75 W mercury lamp and passed through either a 360 nm or a 380 nm filter. The myocytes were stimulated to contract at 0.5 Hz. Fluorescence emissions were detected between 480 nm and 520 nm by a photomultiplier tube after cells were first illuminated at 360 nm for 0.5 s and then at 380 nm for

Table 1
Biometric and echocardiographic parameters of WT and Akt2$^{-/-}$ mice with or with DAS treatment.

Parameter	WT	Akt2$^{-/-}$	DAS	Akt2$^{-/-}$-DAS
Body weight (g)	25.6 ± 0.6	25.3 ± 0.7	24.1 ± 0.4	25.2 ± 0.6
Heart weight (mg)	132 ± 3	137 ± 2	136 ± 3	139 ± 3
Heart/body weight (mg/g)	5.24 ± 0.12	5.44 ± 0.12	5.64 ± 0.20	5.52 ± 0.19
Liver weight (g)	1.15 ± 0.02	1.20 ± 0.03	1.21 ± 0.04	1.23 ± 0.04
Liver/body weight (mg/g)	46.1 ± 1.7	47.6 ± 1.7	50.1 ± 1.5	48.8 ± 1.6
Kidney weight (mg)	343 ± 5	344 ± 5	339 ± 9	332 ± 5
Kidney/body weight (mg/g)	13.7 ± 0.4	13.7 ± 0.3	14.1 ± 0.6	13.2 ± 0.4
Blood glucose level (mg/dl)	99.4 ± 3.3	102.0 ± 4.2	95.9 ± 2.8	100.8 ± 3.0
Heart rate (bpm)	456 ± 8	462 ± 10	443 ± 9	451 ± 13
LV wall thickness (mm)	0.80 ± 0.06	0.74 ± 0.13	1.03 ± 0.06	1.03 ± 0.10
LV septal thickness (mm)	0.84 ± 0.04	0.91 ± 0.09	0.88 ± 0.04	0.95 ± 0.07
LV ESD (mm)	1.54 ± 0.12	2.22 ± 0.09*	1.57 ± 0.14	1.61 ± 0.12#
LV EDD (mm)	2.94 ± 0.14	3.44 ± 0.13*	2.90 ± 0.12	3.24 ± 0.24
Factional shortening (%)	47.9 ± 2.5	35.4 ± 1.3*	46.0 ± 3.9	49.9 ± 3.1#

LV: left ventricular; LV ESD: LV end systolic diameter; LV EDD: LV end diastolic diameter; Mean ± SEM, n = 8–9 mice per group.
* $p < 0.05$ *vs.* WT group.
# $p < 0.05$ *vs.* Akt2$^{-/-}$ group.

the duration of the recording protocol (333 Hz sampling rate). The 360 nm excitation scan was repeated at the end of the protocol, and qualitative changes in intracellular Ca^{2+} concentration were inferred from the ratio of the fluorescence intensity at two wavelengths. Intracellular Ca^{2+} decay rate was calculated from single exponential curve fitting [34].

2.7. Electron microscopy

Mouse abdomen and thorax were opened under anesthesia, and the right atrium was incised to allow the release of blood. Perfusion fixation was immediately initiated using a saline washout. Hearts were perfused with 20 ml of warm (37 °C), pH 7.6, PIPES-buffered formaldehyde-glutaraldehyde at ~3 ml/min, followed by 40 ml of the same fixative but chilled to 4 °C. Hearts were removed immediately and left ventricular and interventricular septal tissues were collected from a 2-mm ring sliced from the midventricular region. These were further minced to 1 mm^3. Fixation continued overnight at 4 °C in a 10:1 fluid/tissue ratio. This was followed by rinsing in PIPES buffer + 2% sucrose (pH 7.4) and overnight postfixation in PIPES buffered 1% OsO_4 + 2% sucrose and 1.5% $K_3FE(CN)_6{\cdot}3H_2O$ at room temperature. Tissue blocks were dehydrated through graded ethanol and propylene oxide, embedded in Epon/Araldite, and cured 48 h at 60 °C. Thin sections (silver-gray interference color) were cut on an RMC-MTXL ultramicrotome equipped with a Diatome diamond knife. Sections were collected on naked copper (300-mesh) grids, stained with lead citrate and uranyl acetate (4% in absolute ethanol), and imaged with a Hitachi 7500 transmission electron microscope [39].

2.8. Histological examination

Following anesthesia, hearts were excised and immediately placed in 10% neutral-buffered formalin at room temperature for 24 h after a brief rinse with PBS. The specimen were embedded in paraffin, cut in 5 µm sections and stained with hematoxylin and eosin (H&E). Cardiomyocyte cross-sectional areas were calculated on a digital microscope (×400) using the Image J (version1.34S) software [34].

2.9. Intracellular fluorescence measurement of superoxide (O_2^-)

Intracellular O_2^- was monitored by changes in fluorescence intensity resulting from intracellular probe oxidation [36]. In brief, cardiomyocytes were loaded with dihydroethidium (DHE, 5 µM) (Molecular Probes, Eugene, OR, USA) for 30 min at 37 °C and washed with PBS buffer. Cells were sampled randomly using an Olympus BX-51 microscope equipped with an Olympus MagnaFire™ SP digital camera and ImagePro image analysis software (Media Cybernetics, Silver Spring, MD, USA). Fluorescence was calibrated with InSpeck microspheres (Molecular Probes). An average of 100 cells was evaluated using the grid crossing method in 15 visual fields per isolation.

2.10. Western blot analysis

Myocardial protein was prepared as described [40]. Samples containing equal amount of proteins were separated on 10% SDS-polyacrylamide gels in a minigel apparatus (Mini-PROTEAN II, Bio-Rad) and transferred to nitrocellulose membranes. The membranes were blocked with 5% milk in TBS-T, and were incubated overnight at 4 °C with anti-NLRP3 (1:1000), anti-iNOS (1:1000), anti-LC3B (1:1000), anti-p62 (1:1000), anti-Pink1 (1:1000), anti-Parkin (1:1000), and anti-B-cell lymphoma 2 (Bcl-2)/adenovirus E1B 19 kDa interacting protein 3 (BNIP3, 1:1000) antibodies. All antibodies were obtained from Cell Signaling Technology (Beverly, MA, USA). After immunoblotting, the film was scanned and the intensity of immunoblot bands was detected with a Bio-Rad Calibrated Densitometer. GAPDH was used as the loading control.

2.11. Neonatal cardiomyocyte (NCM) isolation

Neonatal (1–2 day-old) WT and Akt2$^{-/-}$ mice were sterilized with 75% ethanol before hearts were harvested and rinsed. Small pieces of hearts were digested 4–5 rounds using 0.25% trypsin (Carolina, Burlington, NC, USA). For each round, heart tissues were incubated with 2–4 ml of trypsin at 37 °C for 10 min. Supernatants were neutralized in DMEM medium containing fetal bovine serum (20%), 1% penicillin and streptomycin (Gibco, Grand Island, NY, USA) to terminate the digestion. Cells were centrifuged at 800 ×g for 10 min and pellets were resuspended in DMEM medium containing fetal bovine serum (20%) with 1% penicillin and streptomycin prior to plating in an uncoated dish for 1 h at 37 °C. Cardiomyocytes were plated in a confocal plate pre-coated with 1% gelatin, and cultured for 48 h at 37 °C in the presence of 95% O_2 and 5% CO_2 [41,42].

2.12. LC3B-GFP-adenoviral transfection and assessment of mitophagy

NCM from WT and Akt2$^{-/-}$ mice were transfected with GFP-LC3B adenovirus for 24 h [42] and were treated with or without with diallyl sulfide (100 µM) [37] at 37 °C for 6 h in the absence or presence of the specific NLRP3 activator nigericin (20 µM) [38]. After treatment, cells were rinsed with PBS 3 times and were incubated with MitoTracker

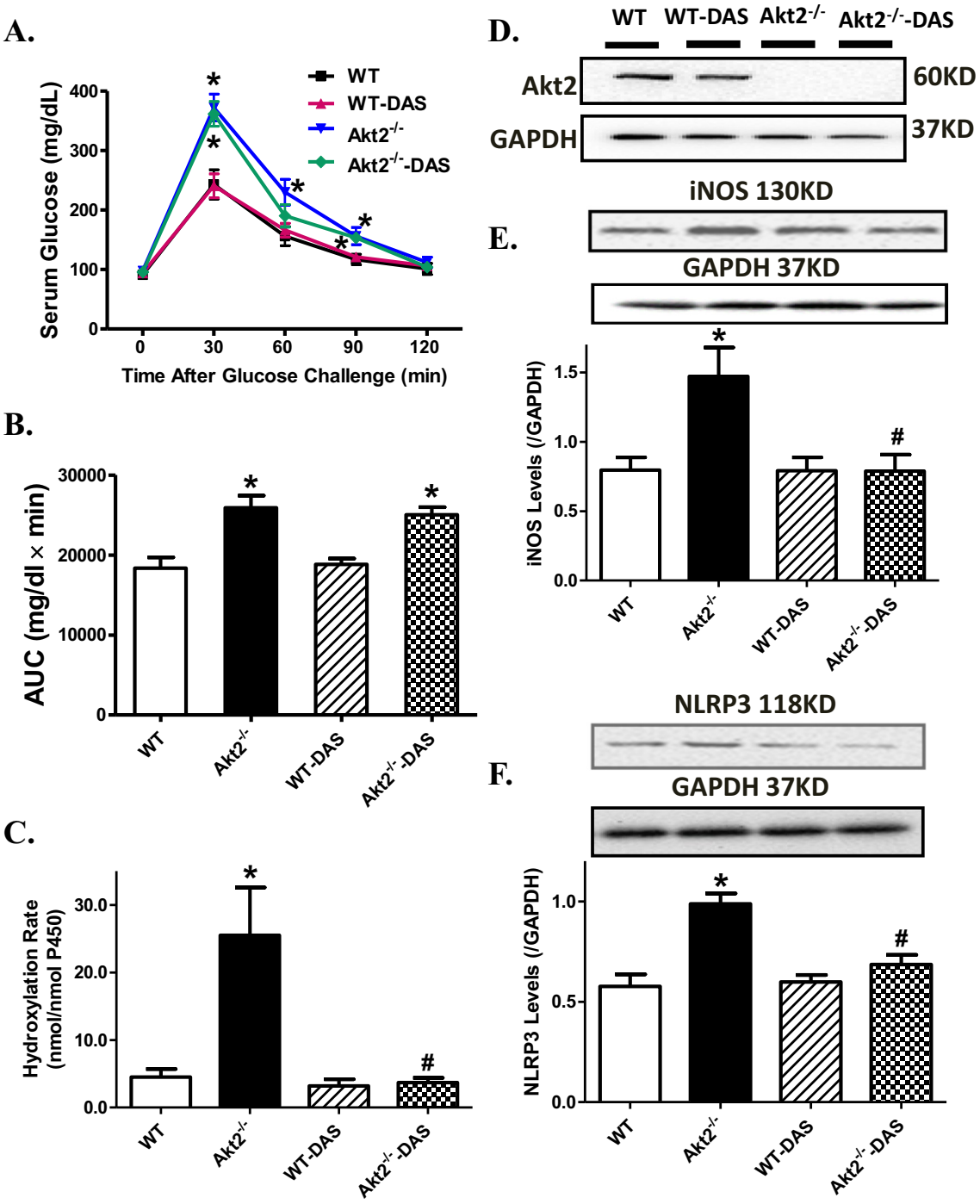

Fig. 1. Effect of the CYP2E1 inhibitor diallyl sulfide (DAS, 100 mg/kg/d, i.p., for 4 weeks) on Akt2 knockout-induced glucose tolerance, changes in myocardial cytochrome P450 2E1 activity, iNOS and inflammasome NLRP3 levels. A. IPGTT curve; B. Area underneath the IPGTT curve in WT and Akt2$^{-/-}$ mice; C: Cytochrome P450 2E1 activity measured by hydroxylation rate in 30 min; D: Akt2 levels; E: iNOS levels; and F: NLRP3 levels. Insets: Representative gels depicting levels of Akt2, iNOS and NLRP3 using specific antibodies (GAPDH as loading control). Mean ± SEM, n = 6–7 mice per group, * $p < 0.05$ *vs.* WT group, # $p < 0.05$ *vs.* Akt2$^{-/-}$ group.

Deep Red (Cell Signaling Technology, Danvers, MA, USA) at a concentration of 500 nM for 30 min at 37 °C. Following incubation, cells were rinsed with PBS and fixed in 4% paraformaldehyde for 15 min at room temperature. Cells were rinsed again with PBS and stained with DAPI at a concentration of 5 μM for 5 min at room temperature. For mitophagy visualization, cells were imaged through the Zeiss 710 Confocal Microscope (Oberkochen, Germany) at ×40 magnification and numbers of GFP-LC3 puncta colocalized with MitoTracker per cell were counted. Images were analyzed using ImageJ software. Data were performed in 5 independent experiments.

2.13. Data analysis

Data are Mean ± SEM. Difference was calculated by repeated measures analysis of variance (ANOVA) followed by a Tukey's *post hoc* analysis. A p value < 0.05 was considered significant.

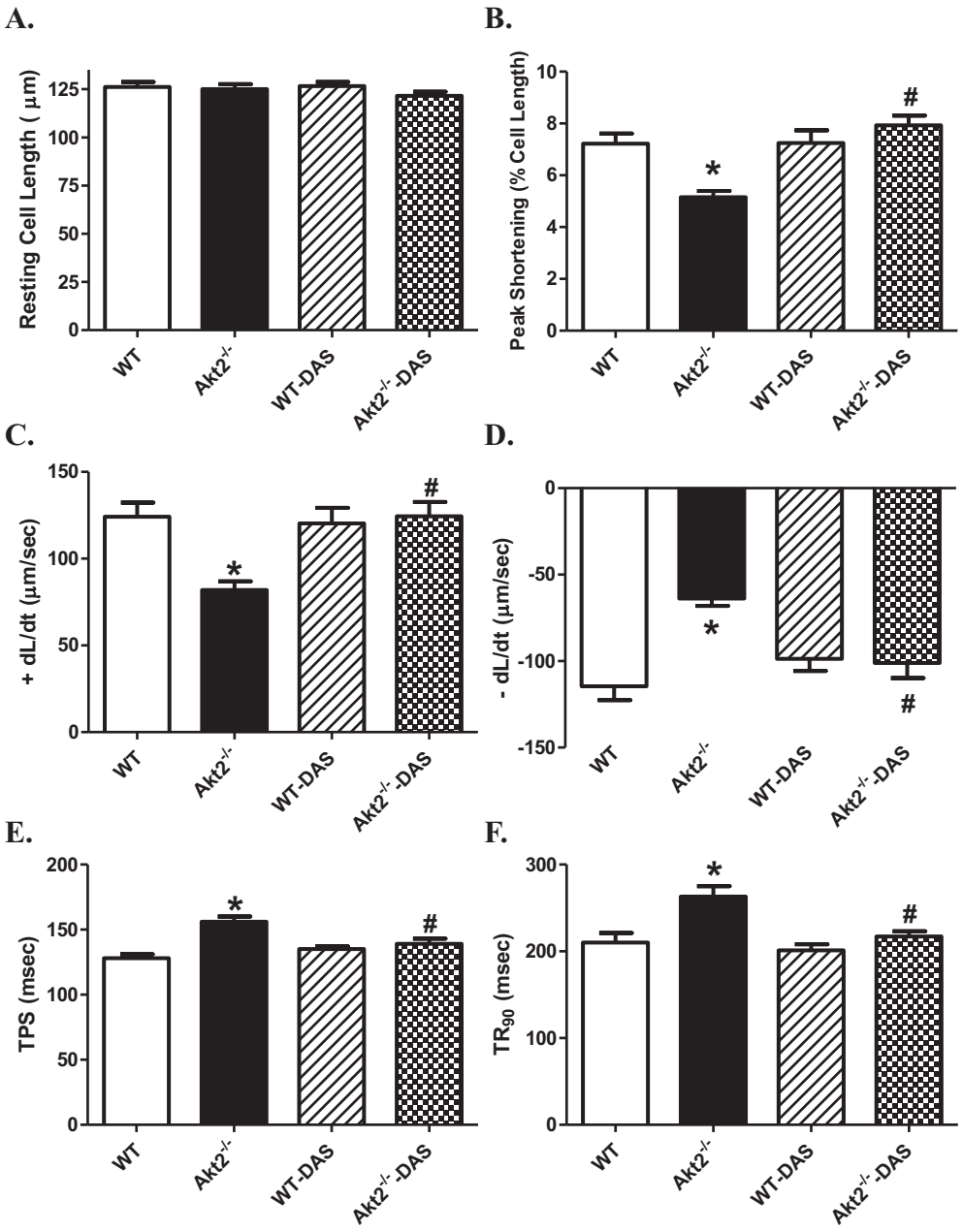

Fig. 2. Effect of the CYP2E1 inhibitor diallyl sulfide (DAS, 100 mg/kg/d, i.p., for 4 weeks) on Akt2 knockout-induced cardiomyocyte contractile dysfunction. A: Resting cell length; B: Peak shortening (PS, normalized to cell length); C: Maximal velocity of shortening (+ dL/dt); D: Maximal of relengthening (− dL/dt); E: Time-to-PS (TPS) and F: Time-to-90% relengthening (TR_{90}). Mean ± SEM, $n = 113$ cells from 5 mice per group, * $p < 0.05$ *vs.* WT group, # $p < 0.05$ *vs.* $Akt2^{-/-}$ group.

3. Results

3.1. General biometric, IPGTT and echocardiographic features of WT and $Akt2^{-/-}$ mice treated with or without diallyl sulfide

Neither Akt2 knockout nor diallyl sulfide treatment overtly affected blood glucose levels, body and organ weights or organ size (organ-to-body weight ratio). Heart rate, left ventricular wall thickness and septal thickness were unaffected by Akt2 or diallyl sulfide treatment, or both. Akt2 knockout significantly enlarged LV EDD and LV ESD as well as suppressed fractional shortening, the effects of which were obliterated by CYP2E1 inhibition. Diallyl sulfide itself did not elicit any notable effect on echocardiographic properties (Table 1). Following intraperitoneal glucose challenge, blood glucose rose quickly in WT and $Akt2^{-/-}$ mice peaking at 30 min and returning to near baseline after 120 min. However, the post-challenge glucose levels achieved significantly higher values between 30 and 90 min in $Akt2^{-/-}$ mice, indicating poor glucose clearance capacity. Diallyl sulfide treatment did not overtly affect the pattern of glucose clearance or AUC in WT or $Akt2^{-/-}$ groups (Fig. 1A–B). Our further analysis revealed that Akt2 ablation overtly increased myocardial CYP2E1 activity, levels of iNOS and inflammasome NLRP3, the effects of which were ameliorated by diallyl sulfide. CYP2E1 inhibitor itself did not elicit any effect on these parameters in WT mice (Fig. 1C, E, F). Akt2 ablation was confirmed using Western blot, the effect of which was unaffected by diallyl sulfide treatment (Fig. 1D).

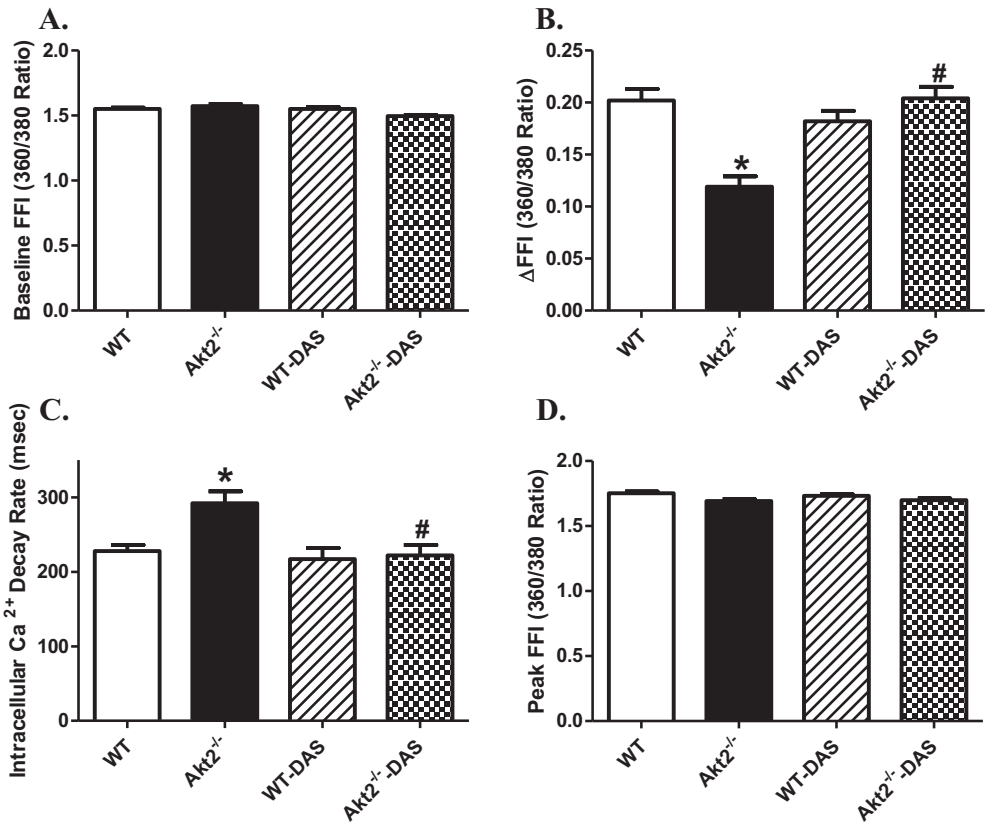

Fig. 3. Effect of the CYP2E1 inhibitor diallyl sulfide (DAS, 100 mg/kg/d, i.p., for 4 weeks) on Akt2 knockout-induced intracellular Ca^{2+} handling derangement. A: Resting fura-2 fluorescence intensity (FFI); B: Electrically-stimulated rise in FFI (ΔFFI); C: Intracellular Ca^{2+} decay rate; and D: Peak FFI; Mean ± SEM, $n = 93$ cells from 5 mice per group, * $p < 0.05$ *vs.* WT group, # $p < 0.05$ *vs.* $Akt2^{-/-}$ group.

3.2. Effect of CYP2E1 inhibition on insulin resistance-elicited changes in cardiomyocyte contractile and intracellular Ca^{2+} properties

Neither Akt2 ablation nor diallyl sulfide treatment, or both, significantly affected the resting cell length. At 10 months of age, Akt2 ablation significantly reduced PS and ± dL/dt as well as prolonged TPS and TR_{90}, the effects of which were abolished by the CYP2E1 inhibitor. Diallyl sulfide itself did not elicit any notable effect on cardiomyocyte contractile mechanics (Fig. 2). To better discern the potential mechanism(s) behind CYP2E1 inhibition-offered beneficial myocardial effects against insulin resistance, Fura-2 fluorescence was examined to assess intracellular Ca^{2+} handling properties. Our data shown in Fig. 3 revealed that cardiomyocytes from $Akt2^{-/-}$ mice exhibited an overtly depressed rise in intracellular Ca^{2+} in response to electrical stimulus (ΔFFI) and prolonged intracellular Ca^{2+} decay although baseline and peak intracellular Ca^{2+} levels were not significantly affected by Akt2 ablation. Although diallyl sulfide itself did not affect intracellular Ca^{2+} properties, it abrogated Akt2 deletion-induced changes in ΔFFI and intracellular Ca^{2+} decay.

3.3. Effect of diallyl sulfide on Akt2 ablation-induced changes in ultrastructure, O_2^- production and histology in murine hearts

To assess the impact of diallyl sulfide on myocardial ultrastructure, oxidative stress and histology under Akt2 ablation-induced insulin resistance, transmission electron microscopy (TEM) was employed to assess the ultrastructure in left ventricles. Our data revealed cytoarchitectural damage as manifested by mitochondrial swelling and overtly disrupted sarcomeres and myofilament array in myocardial tissue sections from $Akt2-/-$ mice, the effect of which was ameliorated by diallyl sulfide treatment. There was essentially little difference in myocardial ultrastructure in myocardial sections between diallyl sulfide-treated and untreated WT groups. Our data also noted enhanced myocardial O2– production in cardiomyocytes from $Akt2^{-/-}$ mice, the effect of which was also reversed by diallyl sulfide with little effect from the CYP2E1 inhibitor itself. Findings from H&E staining revealed that neither Akt2 ablation nor CYP2E1 inhibition (or both), overtly affected cardiomyocyte transverse cross-section area (Fig. 4).

3.4. Effect of diallyl sulfide on insulin resistance-induced changes in autophagy and mitophagy

To explore the possible mechanism underlying diallyl sulfide and/or Akt2 ablation-induced changes in cardiac contractile and intracellular Ca^{2+} function, western blot was employed to assess the levels of protein markers for autophagy and mitophagy. Our data shown in Fig. 5 revealed that Akt2 ablation overtly decreased LC3BII-to-LC3I ratio, Pink1 and Parkin levels, and upregulated the levels of p62 without affecting the levels of BNIP3. Although the CYP2E1 inhibitor itself did not alter levels of these autophagy or mitophagy protein markers, it negated insulin resistance-induced changes in LC3B, p62, Pink1 and Parkin with little effect by itself (Fig. 5).

3.5. Role of NLRP3 in Akt2 deletion-induced changes in cardiomyocyte mitophagy, GFP-LC3B-mitochondrial colocalization and cardiomyocyte mechanical function

To discern the up- and down-stream relationship among NLRP3, mitophagy and CYP2E1 in insulin resistance-induced cardiomyocyte anomalies, we re-examined cardiomyocyte contractile responses and mitophagy protein marker Parkin in the absence or presence of the NLRP3 activator nigericin. Resulted depicted in Fig. 6A revealed that NLRP3 activation nullified diallyl sulfide-induced restoration of Parkin levels in Akt2 knockout group. Nigericin itself did not significantly affect the levels of Parkin. This received support from the cardiomyocyte contractile function evaluation where nigericin cancelled off the beneficial effect of diallyl sulfide on cardiomyocyte contraction in the face of Akt2 deletion. Diallyl sulfide treatment corrected Akt2 deletion-

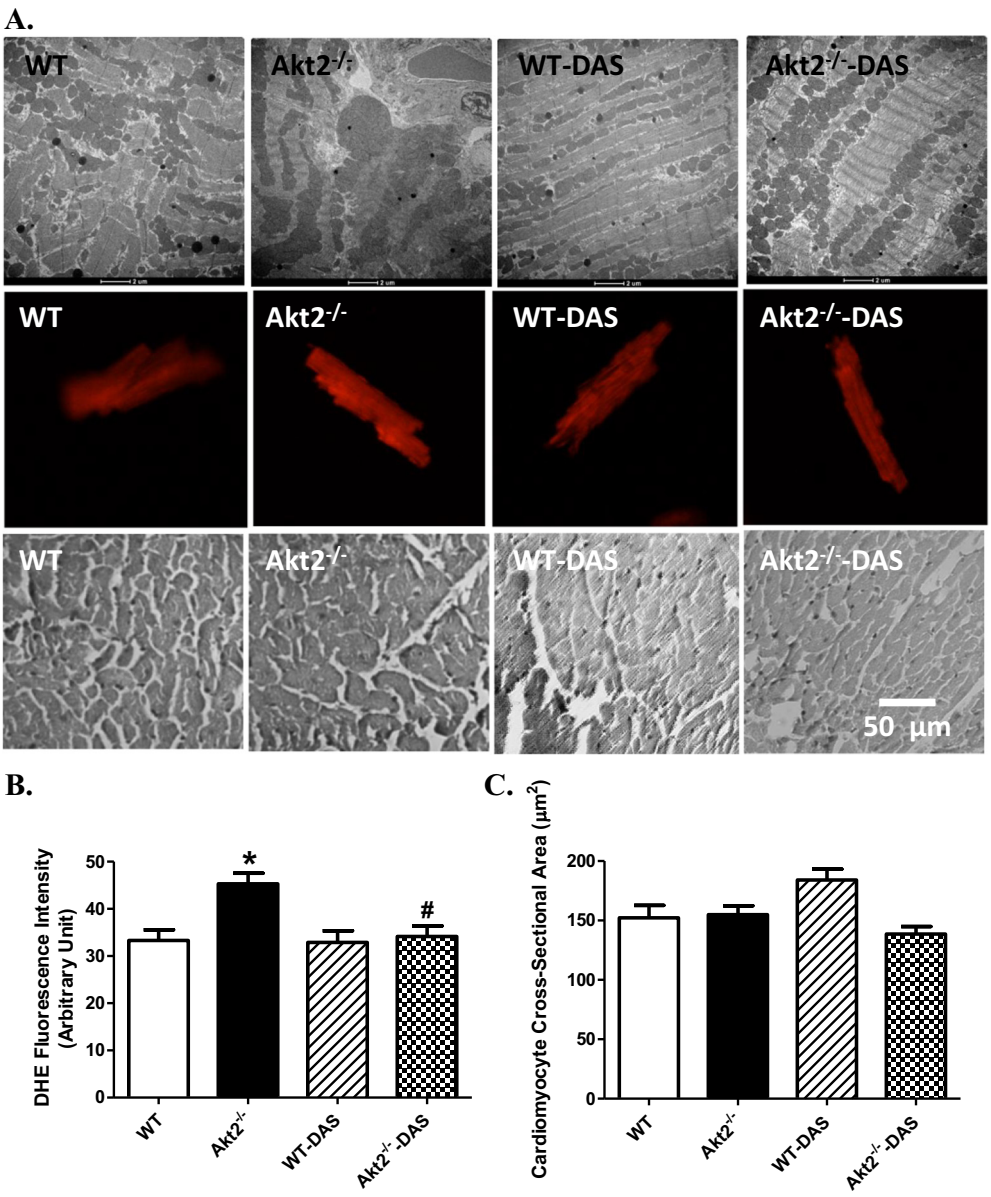

Fig. 4. Effect of the CYP2E1 inhibitor diallyl sulfide (DAS, 100 mg/kg/d, i.p., for 4 weeks) on Akt2 knockout-induced changes in ultrastructure, superoxide (O_2^-) production and cardiomyocyte histology. A: Representative TEM ultrastructural images (× 6000, top panel), DHE fluorescence staining depicting O_2^- production (middle panel) and H&E staining denoting cross-sections of left ventricles (× 200, lower panel); B: Quantitative analysis of O_2^- production in cardiomyocytes; and C: Quantitative analysis of cross-sectional area; Mean ± SEM, $n = 15–16$ (DHE staining) or 9 (H&E staining) microscopic fields per group. * $p < 0.05$ *vs.* WT group, # $p < 0.05$ *vs.* Akt2$^{-/-}$ group.

induced depression in peak shortening and ± dL/dt as well as prolongation of TPS and TR_{90} without affecting resting cell length, the effect of which was absent in the presence of nigericin (Fig. 6B–F). The effect of NLRP3 activation and CYP2E1 inhibition on Akt2 ablation-induced changes in mitophagy was also evaluated in neonatal murine cardiomyocytes using GFP-LC3B-mitochondria colocalization. Our data shown in Fig. 7 revealed that diallyl sulfide effectively ameliorated Akt2 ablation-induced loss in the colocalization of GFP-LC3B and mitochondria (labelled with MitoTracker Red), the effect of which was negated by the NLRP3 activator nigericin.

3.6. Role of iNOS and mitochondrial ROS in Akt2 deletion-induced changes in NLRP3

To determine the correlation among iNOS, mitochondrial O_2^- production and NLRP3 activation, levels of NLRP3 were examined in murine cardiomyocytes from WT and Akt2 −/− mice incubated with or without the iNOS inhibitor SEITU (1 μM) or the mitochondrial ROS scavenger MitoQ (2 μM) for 6 h. Resulted shown in Fig. 8 revealed that iNOS inhibition but not mitoQ negated Akt2 deletion-induced upregulation of NLRP3. Neither inhibitor exerted any notable effect on the levels of NLRP3 themselves.

4. Discussion

The salient findings from our study revealed that CYP2E1 inhibition rescued against myocardial contractile dysfunction, intracellular Ca^{2+} mishandling, mitochondrial ultrastructural damage, deranged autophagy and Pink1-Parkin-mediated mitophagy in Akt2$^{-/-}$ model of insulin resistance. Our data observed elevated cardiomyocyte O_2^- production, upregulated levels of iNOS and NLRP3 along with unaltered cardiac geometry (heart weight, size and cardiomyocyte cross-sectional area) in Akt2$^{-/-}$ murine hearts, the effects of which were reversed or significantly attenuated by diallyl sulfide, suggesting a possible role of oxidative stress, iNOS and NLRP3 inflammasome in CYP2E1 inhibition-elicited beneficial myocardial effect against insulin resistance. Furthermore, our *in vitro* findings further validated a role of iNOS-NLRP3 signaling cascades in Akt2$^{-/-}$ insulin resistance-elicited cardiac anomalies. Taken together, these findings revealed, for the first time, that Akt2 insufficiency may contribute to the development of metabolic cardiomyopathy through a CYP2E1-mediated mechanism, indicating the therapeutic potential of CYP2E1 in the management of metabolic

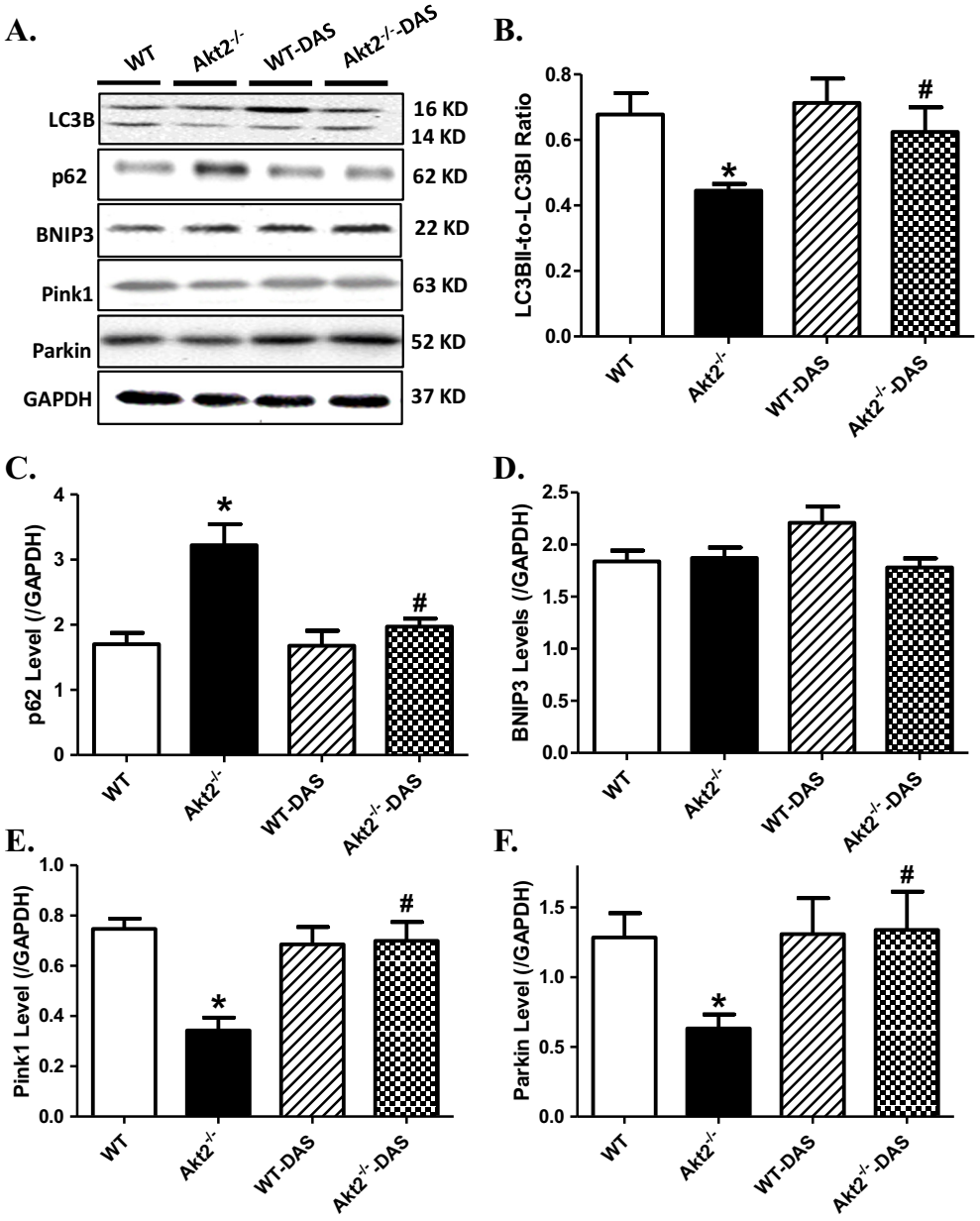

Fig. 5. Effect of the CYP2E1 inhibitor diallyl sulfide (DAS, 100 mg/kg/d, i.p., for 4 weeks) on Akt2 knockout-induced changes in myocardial autophagy and mitophagy. A: Representative gels depicting autophagy and mitophagy protein markers using specific antibodies. GAPDH was used as the loading control; B: LC3BII-to-LC3BI ratio; C: p62 levels; D: BNIP3 levels; E: Pink1 levels; and F: Parkin levels. Mean ± SEM, n = 6–9 mice per group, * $p < 0.05$ *vs.* WT group, # $p < 0.05$ *vs.* Akt2$^{-/-}$ group.

cardiomyopathy.

Observations from our study revealed that prolonged Akt2 ablation triggered insulin resistance, cardiac contractile anomalies (decreased fractional shortening, peak shortening, ± dL/dt, prolonged TPS and TR_{90}), intracellular Ca^{2+} derangement, and oxidative stress, in a manner similar to our previous reports using Akt2$^{-/-}$ or sucrose-fed insulin resistant models [31,34,43,44]. Akt2 knockout elicited cardiac contractile dysfunction in the absence of overt change in cardiac geometry (heart weight, size, resting cell length or cardiomyocyte cross-sectional area), consistent with previous reports using the same or other models of insulin resistance [31,34,44]. The intracellular Ca^{2+} results indicated that cardiac mechanical anomalies in Akt2$^{-/-}$ mice may be underscored by intracellular Ca^{2+} defects (decreased ΔFFI and delayed intracellular Ca^{2+} decay), in line with the earlier notion of impaired intracellular Ca^{2+} homeostasis in insulin resistance [9,31,34,44]. In our hands, Akt2 ablation-induced insulin resistance provoked increased CYP2E1 activity, expression of iNOS and NLRP3 as well as mitochondrial ultrastructural damage as evidenced by swollen mitochondria, loss of sarcomere and myofilament array. Upregulation of iNOS is a common denominator in insulin resistance and cardiovascular sequelae [28]. Upregulation of iNOS is tied with increased mitochondrial damage and ROS production [27,28], and more recently, with activation of NLRP3 inflammasome [29,30]. Increase in iNOS is associated with oxidative stress, macrophage recruitment, upregulated NLRP3 inflammasome, en route to obesity-associated adipose tissue inflammation [30].

Perhaps the most striking of findings from our study was that CYP2E1 inhibition negated insulin resistance-induced myocardial, cardiomyocyte contractile and intracellular Ca^{2+} defects, O_2^- production and mitochondrial damage. Our study suggested that CYP2E1 inhibition is capable of retarding or reversing the progression of insulin resistance cardiomyopathy. Several mechanisms may contribute to the

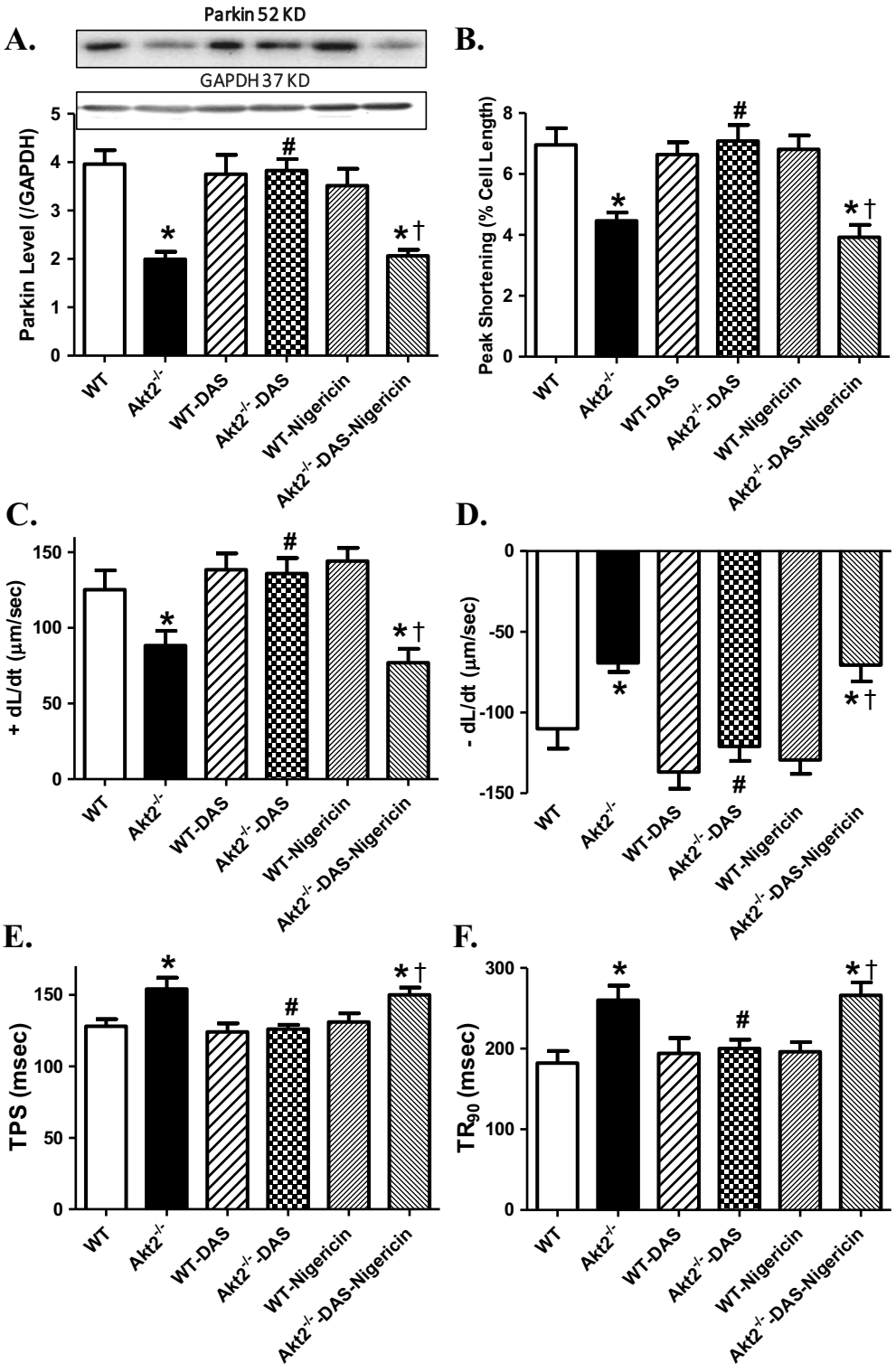

Fig. 6. Effect of the CYP2E1 inhibitor diallyl sulfide (DAS, 100 μM, for 6 h) on Akt2 knockout -induced changes in Parkin levels and cardiomyocyte mechanical function *in vitro* in the presence or absence of the NLRP3 activator nigericin (20 μM). A: Levels of Parkin, Inset: Representative gel bots depicting levels of Parkin and GAPDH (loading control) using specific antibodies; B: Peak shortening (PS, normalized to cell length); C: Maximal velocity of shortening (+ dL/dt); D: Maximal of relengthening (− dL/dt); E: time-to-PS (TPS) and F: Time-to-90% relengthening (TR_{90}). Mean ± SEM, $n = 48$ cells from 2 mice per group, * $p < 0.05$ *vs.* WT group, # $p < 0.05$ *vs.* $Akt2^{-/-}$ group, † $p < 0.05$ *vs.* $Akt2^{-/-}$-DAS group.

beneficial effects of diallyl sulfide against Akt2 knockout-induced metabolic cardiomyopathy. First, diallyl sulfide may likely exert its beneficial effects through alleviating O_2^- production. CYP2E1 inhibition was previously shown to resist alcohol intake-induced oxidative stress and cardiac dysfunction [45]. Second, preserved autophagy, in particular, mitochondrial autophagy, may play an important role in CYP2E1-offered cardioprotection in insulin resistance. Our data revealed that Akt2 ablation suppressed protein markers for autophagy and mitophagy including LC3B, Pink1, and Parkin as well as promoted p62 accumulation as well as GFP-LC3B-mitochondria colocalization, the effect of which was restored by diallyl sulfide. Insulin resistance has been shown to compromise autophagy in the heart [9,46]. Deletion of Atg7 in cardiac and skeletal muscles ameliorated exercise-induced sensitization of insulin signaling, consolidating the role of autophagy in insulin sensitivity [47]. Maintenance of mitochondrial homeostasis through autophagy, in particular mitophagy, by way of removing aged or damaged mitochondria govern mitochondrial function and insulin sensitivity [48]. Our data revealed reduced O_2^- production in $Akt2^{-/-}$

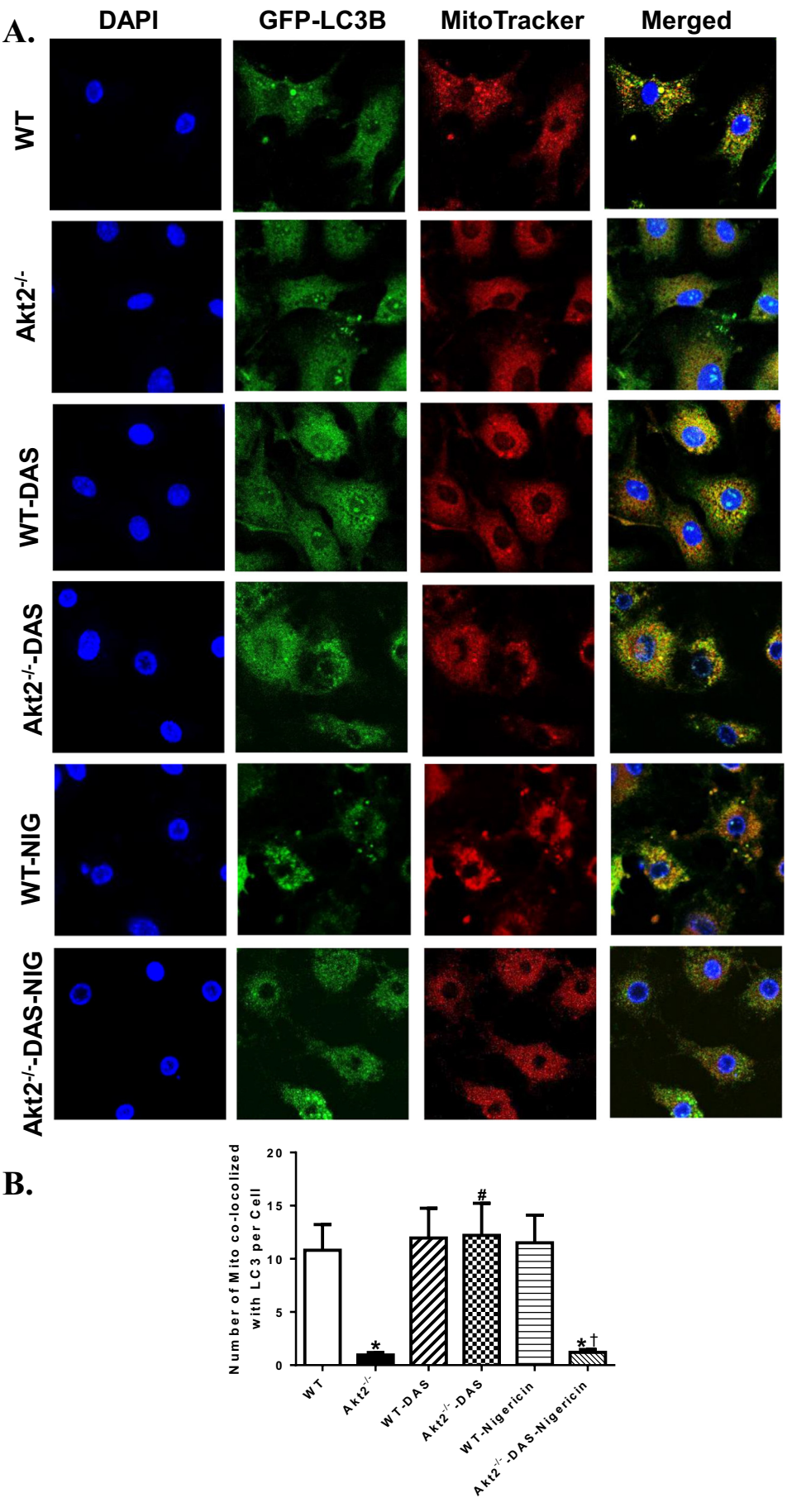

Fig. 7. Effect of the CYP2E1 inhibitor diallyl sulfide (DAS, 100 μM, for 6 h) on Akt2 knockout -induced change in mitophagy assessed by GFP-LC3B-mitochondria colocalization in neonatal murine cardiomyocytes *in vitro* in the presence or absence of the NLRP3 activator nigericin (NIG, 20 μM). A: Representative confocal images (40 ×) of DAPI (blue), GFP-LC3B (green) and mitochondria (MitoTracker) (red) depicting colocalization of GFP-LC3B and mitochondria; and B: Quantitative analysis of GFP-LC3B puncta colocalization with mitochondria (MitoTracker) per cell. Mean ± SEM, $n = 5$ independent experiments per group, * $p < 0.05$ *vs.* WT group, # $p < 0.05$ *vs.* $Akt2^{-/-}$ group, † $p < 0.05$ *vs.* $Akt2^{-/-}$-DAS group.)

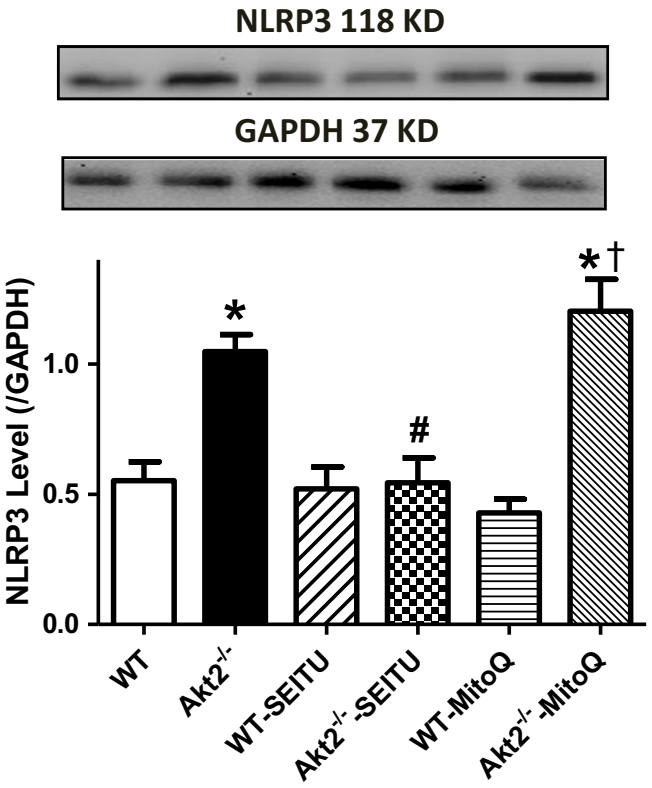

Fig. 8. Effect of the iNOS inhibitor S-ethyl-isothiourea (SEITU) and mitochondrial ROS scavenger mitoQ on Akt2 knockout-induced changes in NLRP3 levels. Murine cardiomyocytes from WT and Akt2$^{-/-}$ mice were incubated with SEITU (1 μM) or MitoQ (2 μM) for 6 h prior to assessment of NLRP3 levels using Western blot analysis. Insets: Representative gels depicting NLRP3 and GAPDH (loading control) levels in murine cardiomyocytes using specific antibodies. Mean ± SEM, $n = 6$ isolations per group, * $p < 0.05$ *vs.* WT group, # $p < 0.05$ *vs.* Akt2$^{-/-}$ group, † $p < 0.05$ *vs.* Akt2$^{-/-}$-SEITU group,

group following diallyl sulfide treatment, in line with preserved mitophagy and mitochondrial ultrastructure. Third, findings from our present work revealed a role of NLRP3 inflammasome in Akt2 ablation- and diallyl sulfide-induced mitophagy and mechanical responses in cardiomyocytes. Activation of NLRP3 nullified diallyl sulfide-induced protective actions against Akt2 ablation-induced unfavorable effects on cardiac mitophagy (protein markers and GFP-LC3B-mitochondria co-localization) and mechanical function, suggesting a permissive role of NLRP3 in CYP2E1 inhibition-offered cardiac benefit. NLRP3 has emerged as an unexpected marker of cardiometabolic stress and is tightly controlled by mitophagy [49]. Our *in vitro* data convincingly suggested that NLRP3 may also serve as an upstream regulator for Parkin-mediated mitophagy and is regulated by iNOS but unlikely mitochondrial ROS in Akt2$^{-/-}$ insulin resistance model. Our results received support from a recent report using human mononuclear cells and mouse macrophage cell line (J774) suggesting an iNOS-mediated regulation of NLRP3 [29]. Activation of NLRP3 has been shown to promote mitochondrial damage through inhibiting mitophagy by way of caspase-1 (a downstream target signal for NLRP3)-mediated proteolytic cleavage of Parkin [50].

Experimental limitations: Our present study suffers from a number of limitations. First and perhaps the foremost, diallyl sulfide may produce off-target (CYP2E1 inhibition) effects such as pleiotropic responses involving Nrf2 regulation [22]. Use of other selective CYP2E1 inhibitors will offer better understanding with regards to the effectiveness of CYP2E1 in insulin resistance-induced cardiac anomalies. Next, although DHE is routinely employed as preferred technique and sensor for *in vitro* detection of superoxide (O_2^-), the red fluorescence may also be originated from products derived reactions other than the reaction of O_2^- with DHE including H_2O_2, $ONOO^-$, HOCl and the binding of nuclear DNA with ethidium formed from a two-electron oxidation of DHE [51].

In summary, data from our study provided compelling evidence that CYP2E1 inhibition using diallyl sulfide counteracts insulin resistance-induced myocardial contractile anomalies, intracellular Ca^{2+} mishandling, oxidative stress, loss of autophagy and mitophagy, favoring a role of cytochrome P450 in metabolic cardiomyopathy. CYP2E1 participates in the metabolism of a number of small molecule substrates including ethanol, drugs and carcinogens [52,53] and contributes to the metabolic derangement in metabolic disorders [19–21]. However, how CYP2E1 and other P450 isozymes are induced by pathological stimuli such as insulin resistance, obesity and type 2 diabetes remains unclear, further study is warranted to better elucidate the role of cytochrome P450 and mitophagy in the onset and development of metabolic cardiomyopathy.

Transparency document

The Transparency document associated this article can be found, in online version.

Acknowledgments

None.

Sources of funding

This work was supported in part by Natural Science Foundation of China (81570225, 81260923, 81770261, 81471444 and 8180020218).

Disclosure

None.

References

[1] J. Ren, L. Pulakat, A. Whaley-Connell, J.R. Sowers, Mitochondrial biogenesis in the metabolic syndrome and cardiovascular disease, J Mol Med (Berl) 88 (2010) 993–1001.
[2] F. Louwen, A. Ritter, N.N. Kreis, J. Yuan, Insight into the development of obesity: functional alterations of adipose-derived mesenchymal stem cells, Obes. Rev. 19 (9) (2018) 888–904.
[3] A. Govindsamy, S. Naidoo, M.E. Cerf, Cardiac development and transcription factors: insulin Signalling, insulin resistance, and intrauterine nutritional programming of cardiovascular disease, J Nutr Metab 2018 (2018) 8547976.
[4] M.A. Abdul-Ghani, A. Jayyousi, R.A. Defronzo, N. Asaad, J. Al-Suwaidi, Insulin resistance the link between T2DM and CVD: basic mechanisms and clinical implications, Curr. Vasc. Pharmacol. (2017) (Epub ahead of print).
[5] G. Lastra, C. Manrique, The expanding role of oxidative stress, renin angiotensin system, and beta-cell dysfunction in the cardiometabolic syndrome and Type 2 diabetes mellitus, Antioxid. Redox Signal. 9 (2007) 943–954.
[6] K.K. Koh, C. Oh, M.J. Quon, Does reversal of oxidative stress and inflammation provide vascular protection? Cardiovasc. Res. 81 (2009) 649–659.
[7] D.P. Kao, R.M. Witteles, A. Quon, J.C. Wu, S.S. Gambhir, M.B. Fowler, Rosiglitazone increases myocardial glucose metabolism in insulin-resistant cardiomyopathy, J. Am. Coll. Cardiol. 55 (2010) 926–927.
[8] G.S. Hotamisligil, Endoplasmic reticulum stress and the inflammatory basis of metabolic disease, Cell 140 (2010) 900–917.
[9] G. Jia, M.A. Hill, J.R. Sowers, Diabetic cardiomyopathy: an update of mechanisms contributing to this clinical entity, Circ. Res. 122 (2018) 624–638.
[10] B. Dummler, B.A. Hemmings, Physiological roles of PKB/Akt isoforms in development and disease, Biochem. Soc. Trans. 35 (2007) 231–235.
[11] N.R. Leslie, The redox regulation of PI 3-kinase-dependent signaling, Antioxid. Redox Signal. 8 (2006) 1765–1774.
[12] Q. Yu, F. Gao, X.L. Ma, Insulin says NO to cardiovascular disease, Cardiovasc. Res. 89 (2011) 516–524.
[13] D. Semple, K. Smith, S. Bhandari, A.M. Seymour, Uremic cardiomyopathy and insulin resistance: a critical role for akt? Journal of the American Society of Nephrology : JASN 22 (2011) 207–215.
[14] G.I. Welsh, L.J. Hale, V. Eremina, M. Jeansson, Y. Maezawa, R. Lennon, D.A. Pons, R.J. Owen, S.C. Satchell, M.J. Miles, C.J. Caunt, C.A. McArdle, H. Pavenstadt, J.M. Tavare, A.M. Herzenberg, C.R. Kahn, P.W. Mathieson, S.E. Quaggin, M.A. Saleem, R.J. Coward, Insulin signaling to the glomerular podocyte is critical

for normal kidney function, Cell Metab. 12 (2010) 329–340.
[15] G.L. King, K. Park, Q. Li, Selective insulin resistance and the development of cardiovascular diseases in diabetes: the 2015 Edwin Bierman award lecture, Diabetes 65 (2016) 1462–1471.
[16] S. George, J.J. Rochford, C. Wolfrum, S.L. Gray, S. Schinner, J.C. Wilson, M.A. Soos, P.R. Murgatroyd, R.M. Williams, C.L. Acerini, D.B. Dunger, D. Barford, A.M. Umpleby, N.J. Wareham, H.A. Davies, A.J. Schafer, M. Stoffel, S. O'Rahilly, I. Barroso, A family with severe insulin resistance and diabetes due to a mutation in AKT2, Science 304 (2004) 1325–1328.
[17] H. Cho, J. Mu, J.K. Kim, J.L. Thorvaldsen, Q. Chu, E.B. Crenshaw 3rd, K.H. Kaestner, M.S. Bartolomei, G.I. Shulman, M.J. Birnbaum, Insulin resistance and a diabetes mellitus-like syndrome in mice lacking the protein kinase Akt2 (PKB beta), Science 292 (2001) 1728–1731.
[18] T.H.t. Reynolds, E. Merrell, N. Cinquino, M. Gaugler, L. Ng, Disassociation of insulin action and Akt/FOXO signaling in skeletal muscle of older Akt-deficient mice, Am. J. Phys. Regul. Integr. Comp. Phys. 303 (2012) R1186–R1194.
[19] M. Sarkozy, G. Szucs, V. Fekete, M. Pipicz, K. Eder, R. Gaspar, A. Soja, J. Pipis, P. Ferdinandy, C. Csonka, T. Csont, Transcriptomic alterations in the heart of non-obese type 2 diabetic Goto-Kakizaki rats, Cardiovasc. Diabetol. 15 (2016) 110.
[20] T. Sugizaki, M. Watanabe, Y. Horai, N. Kaneko-Iwasaki, E. Arita, T. Miyazaki, K. Morimoto, A. Honda, J. Irie, H. Itoh, The Niemann-Pick C1 like 1 (NPC1L1) inhibitor ezetimibe improves metabolic disease via decreased liver X receptor (LXR) activity in liver of obese male mice, Endocrinology 155 (2014) 2810–2819.
[21] J. Wang, T. Zhai, Y. Chen, Effects of Honokiol on CYP450 activity and transporter mRNA expression in type 2 diabetic rats, Int. J. Mol. Sci. 19 (2018).
[22] P.S. Rao, N.M. Midde, D.D. Miller, S. Chauhan, A. Kumar, S. Kumar, Diallyl sulfide: potential use in novel therapeutic interventions in alcohol, drugs, and disease mediated cellular toxicity by targeting cytochrome P450 2E1, Curr. Drug Metab. 16 (2015) 486–503.
[23] B.N. Zordoky, M.E. Aboutabl, A.O. El-Kadi, Modulation of cytochrome P450 gene expression and arachidonic acid metabolism during isoproterenol-induced cardiac hypertrophy in rats, Drug Metab. Dispos. 36 (2008) 2277–2286.
[24] K. Nishida, K. Otsu, Inflammation and metabolic cardiomyopathy, Cardiovasc. Res. 113 (2017) 389–398.
[25] D. Jiang, S. Chen, R. Sun, X. Zhang, D. Wang, The NLRP3 inflammasome: role in metabolic disorders and regulation by metabolic pathways, Cancer Lett. 419 (2018) 8–19.
[26] J.W. Yu, M.S. Lee, Mitochondria and the NLRP3 inflammasome: physiological and pathological relevance, Arch. Pharm. Res. 39 (2016) 1503–1518.
[27] S.S. Soskic, B.D. Dobutovic, E.M. Sudar, M.M. Obradovic, D.M. Nikolic, J.D. Djordjevic, D.J. Radak, D.P. Mikhailidis, E.R. Isenovic, Regulation of inducible nitric oxide synthase (iNOS) and its potential role in insulin resistance, Diabetes and Heart Failure, Open Cardiovasc Med J 5 (2011) 153–163.
[28] A. Jovanovic, E. Sudar-Milovanovic, M. Obradovic, S.J. Pitt, A.J. Stewart, S. Zafirovic, J. Stanimirovic, D. Radak, E.R. Isenovic, Influence of a high-fat diet on cardiac iNOS in female rats, Curr. Vasc. Pharmacol. 15 (2017) 491–500.
[29] L.R. Hoyt, M.J. Randall, J.L. Ather, D.P. Depuccio, C.C. Landry, X. Qian, Y.M. Janssen-Heininger, A. van der Vliet, A.E. Dixon, E. Amiel, M.E. Poynter, Mitochondrial ROS induced by chronic ethanol exposure promote hyper-activation of the NLRP3 inflammasome, Redox Biol. 12 (2017) 883–896.
[30] A. Engin, The pathogenesis of obesity-associated adipose tissue inflammation, Adv. Exp. Med. Biol. 960 (2017) 221–245.
[31] N. Hu, M. Dong, J. Ren, Hydrogen sulfide alleviates cardiac contractile dysfunction in an Akt2-knockout murine model of insulin resistance: role of mitochondrial injury and apoptosis, Am. J. Phys. Regul. Integr. Comp. Phys. 306 (2014) R761–R771.
[32] I.P. Grudzinski, A. Frankiewicz-Jozko, J. Bany, Diallyl sulfide—a flavour component from garlic (*Allium sativum*) attenuates lipid peroxidation in mice infected with *Trichinella spiralis*, Phytomedicine 8 (2001) 174–177.
[33] X. Lin, S. Yu, Y. Chen, J. Wu, J. Zhao, Y. Zhao, Neuroprotective effects of diallyl sulfide against transient focal cerebral ischemia via anti-apoptosis in rats, Neurol. Res. 34 (2012) 32–37.
[34] N. Hu, J. Ren, Y. Zhang, Mitochondrial aldehyde dehydrogenase obliterates insulin resistance-induced cardiac dysfunction through deacetylation of PGC-1alpha, Oncotarget 7 (2016) 76398–76414.
[35] S. Kataoka, H. Yasui, M. Hiromura, H. Sakurai, Effect of insulin-mimetic vanadyl sulfate on cytochrome P450 2E1-dependent p-nitrophenol hydroxylation in the liver microsomes of streptozotocin-induced type 1 diabetic rats, Life Sci. 77 (2005) 2814–2829.
[36] Y. Zhang, L. Li, Y. Hua, J.M. Nunn, F. Dong, M. Yanagisawa, J. Ren, Cardiac-specific knockout of ETA receptor mitigates low ambient temperature-induced cardiac hypertrophy and contractile dysfunction, J. Mol. Cell Biol. 4 (2) (2012) 97–107.
[37] N.S. Aberle 2nd, J. Ren, Short-term acetaldehyde exposure depresses ventricular myocyte contraction: role of cytochrome P450 oxidase, xanthine oxidase, and lipid peroxidation, Alcohol. Clin. Exp. Res. 27 (2003) 577–583.
[38] M.E. Heid, P.A. Keyel, C. Kamga, S. Shiva, S.C. Watkins, R.D. Salter, Mitochondrial reactive oxygen species induces NLRP3-dependent lysosomal damage and inflammasome activation, J. Immunol. 191 (2013) 5230–5238.
[39] A.F. Ceylan-Isik, K.K. Guo, E.C. Carlson, J.R. Privratsky, S.J. Liao, L. Cai, A.F. Chen, J. Ren, Metallothionein abrogates GTP cyclohydrolase I inhibition-induced cardiac contractile and morphological defects: role of mitochondrial biogenesis, Hypertension 53 (2009) 1023–1031.
[40] R. Guo, J. Ren, Alcohol dehydrogenase accentuates ethanol-induced myocardial dysfunction and mitochondrial damage in mice: role of mitochondrial death pathway, PLoS One 5 (2010) e8757.
[41] J. Hu, W. Man, M. Shen, M. Zhang, J. Lin, T. Wang, Y. Duan, C. Li, R. Zhang, E. Gao, H. Wang, D. Sun, Luteolin alleviates post-infarction cardiac dysfunction by up-regulating autophagy through Mst1 inhibition, J. Cell. Mol. Med. 20 (2016) 147–156.
[42] S. Wang, W. Ge, C. Harns, X. Meng, Y. Zhang, J. Ren, Ablation of toll-like receptor 4 attenuates aging-induced myocardial remodeling and contractile dysfunction through NCoRI-HDAC1-mediated regulation of autophagy, J. Mol. Cell. Cardiol. 119 (2018) 40–50.
[43] N.D. Roe, E.Y. He, Z. Wu, J. Ren, Folic acid reverses nitric oxide synthase uncoupling and prevents cardiac dysfunction in insulin resistance: role of Ca2+/calmodulin-activated protein kinase II, Free Radic. Biol. Med. 65 (2013) 234–243.
[44] K.K. Hintz, J. Ren, Prediabetic insulin resistance is not permissive to the development of cardiac resistance to insulin-like growth factor I in ventricular myocytes, Diabetes Res. Clin. Pract. 55 (2002) 89–98.
[45] R.H. Zhang, J.Y. Gao, H.T. Guo, G.I. Scott, A.R. Eason, X.M. Wang, J. Ren, Inhibition of CYP2E1 attenuates chronic alcohol intake-induced myocardial contractile dysfunction and apoptosis, Biochim. Biophys. Acta 1832 (2013) 128–141.
[46] Q. Wang, J. Ren, mTOR-independent autophagy inducer trehalose rescues against insulin resistance-induced myocardial contractile anomalies: role of p38 MAPK and Foxo1, Pharmacol. Res. 111 (2016) 357–373.
[47] Z. Yan, A. Kronemberger, J. Blomme, J.A. Call, H.M. Caster, R.O. Pereira, H. Zhao, V.U. de Melo, R.C. Laker, M. Zhang, V.A. Lira, Exercise leads to unfavourable cardiac remodelling and enhanced metabolic homeostasis in obese mice with cardiac and skeletal muscle autophagy deficiency, Sci. Rep. 7 (2017) 7894.
[48] J. Sarparanta, M. Garcia-Macia, R. Singh, Autophagy and mitochondria in obesity and type 2 diabetes, Curr. Diabetes Rev. 13 (2017) 352–369.
[49] M.D. Cordero, M.R. Williams, B. Ryffel, AMP-activated protein kinase regulation of the NLRP3 inflammasome during aging, Trends Endocrinol. Metab. 29 (2018) 8–17.
[50] I. Gkikas, K. Palikaras, N. Tavernarakis, The role of mitophagy in innate immunity, Front. Immunol. 9 (2018) 1283.
[51] M. Yazdani, Concerns in the application of fluorescent probes DCDHF-DA, DHR 123 and DHE to measure reactive oxygen species in vitro, Toxicol. in Vitro 30 ((2015) 578–582.
[52] A.I. Cederbaum, L. Yang, X. Wang, D. Wu, CYP2E1 sensitizes the liver to LPS- and TNF alpha-induced toxicity via elevated oxidative and nitrosative stress and activation of ASK-1 and JNK mitogen-activated kinases, Int J Hepatol 2012 (2012) 582790.
[53] L. Knockaert, B. Fromenty, M.A. Robin, Mechanisms of mitochondrial targeting of cytochrome P450 2E1: physiopathological role in liver injury and obesity, FEBS J. 278 (2011) 4252–4260.